A stress-controlled mechanism for the intensity of very large magnitude explosive eruptions

Article

Accepted Version

A stress-controlled mechanism for the intensity of very large magnitude explosive eruptions

Costa, A.[1], J. Gottsmann[2], O. Melnik[2,3] and R.S.J. Sparks[2]

1. *Environmental Systems Science Centre, University of Reading, Reading, UK, and Istituto Nazionale di Geofisica e Vulcanologia, Naples, Italy.*
2. *Department of Earth Sciences, University of Bristol, Bristol, BS8 1RJ, UK.*
3. *Institute of Mechanics, Moscow State University, Moscow, Russia.*

Abstract

Large magnitude explosive eruptions are the result of the rapid and large-scale transport of silicic magma stored in the Earth's crust, but the mechanics of erupting teratonnes of silicic magma remain poorly understood. Here, we demonstrate that the combined effect of local crustal extension and magma chamber overpressure can sustain linear dyke-fed explosive eruptions with mass fluxes in excess of 10^{10} kg/s from shallow-seated (4-6 km depth) chambers during moderate extensional stresses. Early eruption column collapse is facilitated with eruption duration of the order of few days with an intensity of at least one order of magnitude greater than the largest eruptions in the 20th century. The conditions explored in this study are one way in which high mass eruption rates can be achieved to feed large explosive eruptions. Our results corroborate geological and volcanological evidence from volcano-tectonic complexes such as the Sierra Madre Occidental (Mexico) and the Taupo Volcanic Zone (New Zealand).

1. Introduction

An explosive eruption typically occurs from a vent fed, at shallow depth, by a cylindrical conduit. At greater depth magma is believed to be supplied via dykes, as it is the most efficient means of moving magma through cold lithosphere (Rubin, 1990), and supported from field

evidence (Gudmundsson, 2002) and geophysical analysis (Hautmann et al. 2008; Sigmundsson et al. 2011). Hence, in many eruptions there will be a process of flow localization leading to both spatial and temporal transitions between a dyke and a cylindrical conduit. Explosive volcanic eruptions have hitherto been largely modeled in terms of multiphase flows through rigid conduits of a fixed cross-section, ranging from cylinders to parallel-sided conduits, the latter to simulate dykes. By accounting for wall rock elasticity, Costa et al. (2009) demonstrated that explosive flows of fragmented pyroclastic mixture along elastic dykes showed major differences to results for undeformable conduits. Dyke-like conduits showed a pronounced maximum in underpressure (the difference between the lithostatic pressure and the flow pressure). The underpressure maximum of several tens of MPa occurs at the fragmentation level, where the dyke width is also at a minimum. For some governing parameters the dyke thickness tends to zero and the eruption either stops or the flow localises along a cylindrical geometry. Magma flow through a dyke connected to a shallow cylindrical conduit, during explosive eruptions, is more stable because the fragmentation level moves into the cylindrical part of the conduit where deformation is negligible (Costa et al., 2009). For cylindrical conduits mass fluxes during an eruption are limited by their radii, which commonly are on the order of tens of meters (*e.g.*, Wilson et al., 1980). Calculated fluxes (*e.g.,* Wilson et al., 1980) do not seem high enough to reach the mass fluxes inferred for very large magnitude ignimbrite eruptions (Bryan et al., 2010), although there is a debate as due to the duration of such large eruptions, which in turn determines mass eruption rates (MERs) (Wilson, 2008). Due to the absence of direct observations of very large magnitude eruptions (M≥7) (Mason et. al., 2004) there are large uncertainties associated with both their eruption mechanics and duration.

One way of addressing this problem is to establish the MERs. However, MERs are not well constrained, in part due to the absence of plinian-fall deposits from which eruption column heights are commonly inferred to estimate MER (*e.g.*, Carey and Sparks, 1986). Estimates of

peak MER for the most intensive explosions in the past century (the M6, 1912 Novarupta eruption and the M6 1991 Pinatubo eruption) are between 0.3 and 1.3×10^9 kg/s (Fierstein and Hildreth, 1992; Fierstein and Wilson, 2005; Suzuki and Koyaguchi, 2009).

Methods to assess MER from major ignimbrite eruptions (M>7) are less developed and applied. Sigurdsson and Carey (1989), estimate a minimum MER of around 5×10^8 kg/s for their estimate of ~50 km^3 of magma erupted in the 1815 eruption of Tambora. Self et al. (2004) revised the erupted volume for the same eruption and suggested a volume of 30-33 km^3 and a mean MER of between 8.6 and 9.4×10^8 kg/s, similar to that of Pinatubo 1991. Most very large magnitude explosive eruptions are associated with caldera formation and localisation of magma flow from a ring dyke into multiple conduits from which explosive activity emanates (*e.g.*, Suzuki-Kamata et al., 1993). For example, deposits of the ~770 ka Bishop Tuff eruption document vent migration along a ring fracture and estimates of MER are $\sim4\times10^9$ kg/s (Hildreth and Mahood, 1986; Wilson and Hildreth, 1997). This value is about 4-10 times higher than the peak MER estimates of the Pinatubo 1991 climatic phase. Explosive events with MER well in excess (by up to two orders of magnitude) of those inferred for Plinian eruptions are required to explain veneer deposits and run-out distances from explosive silicic ignimbrite eruptions. Wilson and Walker (1981) estimated $\sim10^{11}$ kg/s for the peak rate of the Taupo eruption, corroborated from observations of run-out and overtopping of mountains by the flow. Furthermore, recent work on giant ash cloud dynamics (Baines and Sparks, 2005), suggests that MER for large ignimbrite eruptions must be $\geq10^{10}$ kg/s.

Eruptions fed directly from dykes along linear fissures could provide a realistic scenario for large magnitude ignimbrite eruptions as a greater cross-section area could result in drastically higher mass eruption rates, provided the dyke remains open over much of its length and it is sustained throughout the entire explosive activity. Very large magnitude fissure-fed effusive basalt eruptions have been documented in Large Igneous Provinces (LIP) (Bryan et al., 2010). Those

flood basalts have MER that are inferred to be 3 to 4 orders of magnitude lower (~10^6 kg/s, Self et al., 1998) than those invoked for explosive felsic supereruptions. However, flood basalt MERs have to be maintained for years to decades in order to emit the huge amounts of lava seen in flood-basalt flow fields. The feasibility and mechanics of feeding explosive silicic ignimbrite eruptions through linear fissures, though postulated to exist (Korringa, 1973; Aguirre-Diaz and Labarthe-Hernañdez, 2003), are largely unexplored. Silicic ignimbrite eruptions are documented in a variety of tectonic settings, including convergent margins and active continental-scale extension. There is, however, circumstantial evidence that "even where they occur in broadly convergent regions, silicic ignimbrite eruptions appear to be commonly and perhaps invariably associated with local extension" (Miller et al., 2008).

Growth of a reservoir of melt-dominant magma exceeding several hundreds of cubic kilometres in volume superimposes a "magmatic" stress field (Gudmundsson, 1988; 1998) on local and regional scales, which either counteracts or adds to dominant tectonic stresses depending on the sign and intensity of the far-field stress and on the magma chamber shape and orientation. During reservoir assembly and magma evolution, the crust typically has to accommodate a magmatic pressure increase (Tait et al., 1989) as well as a significant thermal perturbation (Jellinek and De Paolo, 2003; Rowland et al., 2010), both of which result in a volume increase and would lead to upward doming of surrounding rock. Deviatoric extensional stresses at the free surface result from doming and foster tensile failure at topographic highs as documented by central apical grabens on resurgent domes or in models of caldera formation (Komuro et al., 1984).

Building on Costa et al. (2009), we investigate the effect of extensional stresses on the intensity of explosive silicic eruptions. Here we are concerned with the specific case of explosive

eruptions from a linear fissure similar to, for example, the fissure eruptions of ignimbrite from Southern Sierra Madre Occidental, Mexico (Aguirre-Diaz and Labarthe-Hernañdez, 2003). Our approach is not valid to explain formation and eruption dynamics through ring fissures, as the study of a ring fissure system under an extensional far-field stress would require a full 3D model.

2. Model description

We model eruptions based on the assumption that they are fed by linear dykes that emanate from magma reservoirs (Fig. 1) located at depths of 4 to 8 km (*e.g.,* Smith et al., 2005; Matthews et al., 2011) under extensional far-field stresses. We explore a bandwidth of extensional stresses σ_{ff} from neutral ($\sigma_{ff} = 0$ MPa) to $\sigma_{ff} = 80$ MPa. The higher end of this spectrum characterizes the transition to an active extensional setting (Turcotte and Schubert, 2002), while lower and intermediate values capture local extension induced by a large magma reservoir.

We develop a steady-state model of explosive flows of silicic magma along a linear dyke having an elliptical cross-section with semi-axes a_d and b_d that can change with depth *z* under the effects of both the local magmatic pressure and the net far-field stress (Figure 1). The dyke emanates from the centre of the magma chamber along its *y*-axis. We assume that vertical variations in the cross-section area of the dyke occur at length-scales that are much larger than the dyke width. The model takes into account elastic wall-rock deformation and the governing equations for the cross-section averaged variables equations are here derived as in Costa et al. (2009). The model accounts for the compressibility of both exsolved gas and condensed phases (melt and crystals). Pressure, $P = P_{ch}$, is fixed at the base of the conduit and choked flow conditions are assumed at the top (Macedonio et al., 2005). The magma enters the conduit in either the homogeneous or the bubbly flow regime, and exits in the particulate flow regime, after

125 fragmentation. For simplicity we assume that fragmentation occurs when the gas volume
126 fraction, α, reaches a critical value of 0.75 (Sparks, 1978). However, other choices of
127 fragmentation criterion (Melnik, 1999; Papale, 1999) produce similar results. The flow is
128 assumed isothermal and is described in terms of its mean vertical mixture (melt, bubbles and
129 crystals). For simplicity, magma viscosity is assumed constant. As reference viscosity, here, we
130 consider 10^7 Pa s, which represents a typical value for a silicic magma with more than 40% of
131 crystal, similar to magma characterizing some fissure eruptions from the Southern SMO volcanic
132 system (Gottsmann et al., 2009). In our simulations, the main effect of magma crystallinity is on
133 magma fragmentation depth. At low crystal content, the fragmentation level moves to shallower
134 depth, at higher crystallinity fragmentation occurs at greater depth because the critical volume
135 fraction of bubbles is attained earlier upon magma ascent. Our model is therefore appropriate to
136 apply to magmatic systems with a wide range of crystal contents. However, more realistic
137 descriptions of the effective viscosity (out of the scope of this paper) should account for the
138 coupling with dissolved water, heat loss, viscous dissipation and two-dimensional effects (Costa
139 et al., 2007a).
140
141 Following the assumptions in Costa et al. (2009), the governing mass and momentum equations
142 are:
143 $$\frac{\partial}{\partial z}(\rho A V) = 0 \qquad (1)$$
144 and
145 $$V\frac{\partial V}{\partial z} = -\frac{1}{\rho}\frac{dP}{dz} - g - f_{\mathrm{ft}} \qquad (2)$$
146 where $A = \pi\, a\, b$ is the cross-section area, V is the vertical mixture velocity, g is the gravity
147 acceleration and f_{ft} is the friction term expressed as $f_{\mathrm{ft}} = 4\frac{\mu}{\rho}\frac{a^2+b^2}{a^2b^2}V$ (*e.g.,* Costa et al.,

148 2007b) below the fragmentation level and $f_{\mathrm{ft}} = 0$ above the fragmentation level (μ denotes the
149 magma viscosity, here assumed constant). Assuming a homogeneous mixture, magma density is
150 (*e.g.,* Macedonio et al., 2005):

151 $$\frac{1}{\rho} = \frac{x_e}{\rho_g} + \frac{1 - x_e - x_c}{\rho_l} + \frac{x_c}{\rho_c} \qquad (3)$$

152 where ρ_g is the gas density, x_e is the exsolved gas mass fraction, and x_c is the crystal mass
153 fraction. The exsolved and the dissolved gas mass fraction can be expressed as:

154 $$x_e = \frac{x_{tot} - x_d}{1 - x_d}(1 - x_c); \qquad x_d = s\, P^n \qquad (4)$$

155 where x_{tot} is the initial total gas mass fraction, x_d is the dissolved gas mass fraction; the
156 exponent *n* and the constant *s* in the solubility law are assumed to be independent of pressure,
157 but dependent on the magma composition only (see Table 1).
158 We assume that the gas phase behaves as a perfect gas and the condensed phases are
159 compressible:

160 $$\rho_g = P/(R_g T); \qquad \rho_l = \rho_{l0}(1 + P/\beta) \qquad (5)$$

161 where R_g is the gas constant and T is the temperature; β denotes the bulk modulus of melt
162 (and/or crystals) and it is assumed to be equal to 10 GPa, i.e. similar to values of the typical bulk
163 modulus for host rocks (*e.g.,* Huppert and Woods, 2002).
164 The dyke semi-axes a_d and b_d depend on the difference between magmatic pressure and normal
165 stress in host rocks ΔP (Meriaux and Jaupart, 1995; Costa et al., 2007b; Costa et al., 2009) as
166 follows:

167 $$a_d(z) = a_{d0}(z) + \frac{\Delta P}{2G}\left[2(1-\nu)b_{d0}(z) - (1-2\nu)a_{d0}(z)\right] \qquad (6a)$$

168 $$b_d(z) = b_{d0}(z) + \frac{\Delta P}{2G}\left[2(1-\nu)a_{d0}(z) - (1-2\nu)b_{d0}(z)\right] \qquad (6b)$$

169 $$\Delta P = P - (\rho_r g z - \sigma_t) \qquad (7)$$

Here z denotes the vertical coordinate along the dyke axis, G is the rigidity of wallrock, ν is Poisson's ratio, a_{d0} and b_{d0} are the unpressurized values of the semi-axes. The contribution to the tensile stress along the axis of the conduit σ_t due to the presence of magma chamber with a circular cross-section (having pressure P_{ch} and aspect ratio $a_{ch}/b_{ch} \approx 1$) under the effect of an extensional far-field stress σ_{ff} acting on the plane $x-z$ (see Figure 1), is calculated using the general analytical solutions by Gao (1996) obtained in the limit of a plane 2D geometry (approximation valid for c_{ch} much larger than both a_{ch} and b_{ch}). For the limitations of the model presented above and for detail about the solving methodology see Macedonio et al. (2005) and Costa et al. (2009).

Concerning the solution for the stress field, there are also some simplifications. The medium is assumed to be homogeneous and purely elastic. The solution is valid for an unbounded domain so the effects related to topography, active faults and block boundaries are neglected. Rock stress distribution is affected by presence of pore fluids, temperature and alteration of different layers. The far field stress is assumed to be homogeneous. In application to a particular volcanic system the above effects can be accounted for by means of finite element solvers with appropriate rock properties and boundary conditions (see Hautmann et al., 2009 for a case study of the Soufriere Hills Volcano, Montserrat). This is a first-order study and we keep the rock stress model as simple as possible to capture only general large-scale features. However, in the Appendix we show that the effects of 3D geometry and presence of a free surface on the rock stress distribution do not change the solution significantly and that, within our assumptions, the 2D solution is able to capture correctly the first-order behaviour.

Here, we consider a representative magmatic system with an eruptible chamber volume of $V_{ch} = \pi a_{ch} b_{ch} c_{ch} \simeq 750\ \mathrm{km}^3$. For an average bulk density of crystal-rich magma of 2500 kg/m^3 the corresponding eruptible mass is 1.9×10^{15} kg. ΔP is termed over-pressure for positive values and

195 under-pressure for negative values. All the parameter values are listed in Table 1.

196 In our analytical solution the stress along the dyke depends on the intensity of the extensional
197 stress and on the magma chamber aspect ratio a_{ch}/b_{ch}. For the purpose of this paper, we keep the
198 conduit flow model as simple as possible and focus on evaluation of conditions for an elongated
199 reservoir with a circular cross section (*i.e.*, $a_{ch} = b_{ch} = 4$ km). Although results for chambers with
200 other aspect ratios are different in detail, the results reported herein capture the first-order effects
201 common for all models.

202

203 FIGURE 1 HERE

204

205 **3. Results and discussion**

206 Fig. 2a show the effect of σ_{ff} for the case of a magma chamber at a depth of *L*=6 km with a
207 pressure of 20 MPa (above the lithostatic pressure). For a chamber with a circular cross-section,
208 the stress at the base of the dyke is always greater than the absolute extensional stress σ_{ff}. For an
209 unpressurized magma chamber, the maximum tensile stress at the base of the dyke (*x = 0, z =*
210 b_{ch}) in this case is $\sigma_t = 3\sigma_{ff}$ (Gudmundsson, 1988). There is a critical extensional stress that will
211 produce a tensile stress at the base of the dyke that counterbalances the lithostatic pressure.
212 Under these conditions dykes remain open with maximum length comparable to the elongation
213 of the magma chamber. This has important implications for the intensity of an eruption through a
214 dyke.

215 Using parameters reported in Table 1, Figure 2b shows the effect of extensional stress σ_{ff} on the
216 normalized dyke cross-section profile ($a_d b_d / a_{d0} b_{d0} \approx b_d / b_{d0}$) for a dyke width of $b_{d0} = 5$ m. If
217 the crustal extension is small the dyke tends to remain closed, but if $\sigma_{ff} > 40$ MPa the normalized
218 cross-section remains considerably larger than one and the dyke remains open. There is a sharp

increase in dyke cross-section area if σ_{ff} ≈ 50-60 MPa. Our results show that for a far-field stress above its critical value, *i.e.* the value able to counterbalance the lithostatic pressure at the fragmentation depth, a dyke of any length remains opened; and the MER is controlled by the 3D geometry and extension of the system. For subcritical far-field stresses, the maximum sustainable length of a dyke is strongly controlled by the value of σ_{ff}, length ranges from several hundreds of metres for neutral far-field stress conditions, to few kilometres for σ_{ff} near the critical stress.

FIGURE 2 HERE

These results show that MER strongly depends on the local stress field (Figure 3). Considering a 6 km deep chamber, feeding a dyke with an unpressurized width of $b_{d0} = 5\,\mathrm{m}$, and chamber overpressure (above lithostatic) of 20 MPa, the MER is two order of magnitude greater for a far-field stress of $\sigma_{ff} = 60$ MPa compared with neutral stress conditions.

The effect of magma chamber depth is shown in Figure 3, which gives the solutions for a range of magma chamber depths (4 to 8 km). Shallow chambers require smaller extensional stresses to empty at the same rate as deeper chambers.

FIGURE 3 HERE

Our models indicate that even small to intermediate extensional crustal stresses facilitate the efficient evacuation of a large magmatic reservoir through a dyke. We discuss the role stress plays in the eruption of large volumes of silicic magmas, using the Mid-Tertiary Ignimbrite-flare-up from Sierra Madre Occidental (SMO), Mexico and major ignimbrite eruptions of the Taupo Volcanic Zone, New Zealand as examples.

Aguirre-Diaz and Labarthe-Hernandez (2003) have proposed that a substantial amount of the ~ 400,000 km^3 of silicic magma discharged in the Sierra Madre Occidental (SMO) was channelled from the reservoirs and erupted at the surface along dykes. In their study area in the southern SMO, typical exposed (post-eruption) dykes are up to 10 m wide and tens of meters to several kilometres long. Discontinuous lens-shaped bodies form sets of dykes up to 50 km length, which strike along normal faults. The pyroclastic textures of the dykes and proximal depositional facies of co-ignimbrite lithic-rich lag breccias reflect the interface between the intrusive sub-volcanic and the explosive sub-aerial system and attest to the feeding of these eruption by fissures during continental extension (Bryan et al*.,* 2008). Pyroclastic dykes exposed either side of the Bolaños graben fed the Alacrán ignimbrite (Aguirre-Diaz and Labarthe-Hernandez, 2003), which appears to have been a M7 or M8 event.

An example of an area of current active extension and magma-assisted rifting is the Taupo Volcanic Zone (TVZ) in New Zealand (Reyners, 2010, Rowland et al., 2010, Cole et al., 2010). The TVZ is the source of four M>8 ignimbrite eruptions, namely the ~1.21 Ma Ongatiti, ~1.0 Ma Kidnappers, ~340 ka Whakamaru and ~27 ka Oruanui events (Froggatt et al., 1986; Wilson et al., 2009). Petrological and stratigraphic investigations indicate the upper surface of the Whakamaru magmatic system was at ~5 km (Brown et al., 1998), and suggest a volcano-tectonic trigger for the eruption. There is also evidence for elongate fissure-like structures in the smaller Taupo eruption (Houghton et al. 2010), and in Phase 3 of the Oruanui eruption (Wilson 2001). Work by Wilson (1985) indicates that the M7 Taupo eruption released ~10 km^3 of magma in less than seven minutes, which corresponds to mass eruption rates of order of 10^{10} kg/s. Other evidence for volcano-tectonic interaction comes from the Okataina Volcanic Centre (TVZ) where rhyolitic eruptions occurred from several simultaneously active vents along the Haroharo

linear vent zone (Nairn, 1992; Smith et al., 2006). These geological and volcanological findings are in accord with our results and appear to indicate that at least parts of these eruptions came from linear dyke vents.

Assuming magma storage depths at 6 km, the Alacrán, SMO (100-500 km^3 DRE) and Whakamaru (1500 km^3 DRE; Matthews et al., 2011) ignimbrite would have been erupted within a few days during intermediate extensional stresses. For shallower chambers under similar stresses, the MER can be significantly higher ($>>10^{10}$ kg/s) and eruption duration significantly shorter. Due to the steady-state eruptive conditions considered by our models, however, the inferred eruption durations must be regarded as lower bound values.

High intensity explosive eruptions, MER > 5×10^9 kg/, favour conditions for column collapse and generation of pyroclastic flows instead of a plinian eruption column (Wilson et al., 1980; Woods and Bower, 1995). Because of their large cross-sectional area (Fig. 2b), explosive flow through dykes promotes similar conditions for column collapse early on in eruptions. This is consistent with the observed generally smaller volumes of Plinian fall deposits compared with volumes of pyroclastic density current deposits (welded and rheomorphic; Bryan et al., 2008; Gottsmann et al., 2009). Rapid initial rifting at peak chamber pressure may be one explanation for this observation. Our analysis indicates that high intensity, large-scale eruptions of deep-seated (> 8 km) magma are not typically controlled by extensional stresses. To explain the >M9 high-Ti-type silicic eruptions fed by inferred lower crustal magma chambers reported from the Paraná-Etendeka LIP (Bryan et al., 2010) requires either significantly higher (catastrophic?) extensional stresses than those considered here, or other eruptive mechanisms altogether.

4. Conclusions

We have made significant progress towards explaining the mechanical conditions for very high mass discharge rates characterizing major ignimbrite eruptions along linear fissures, corroborating geological evidence and other ways of inferring MERs. Our results show that MERs in excess of 10^{10} kg/s are readily attainable under moderate extensional stresses from such fissures. Our model captures the first order controls of linear fissure-fed eruptions indicating a substantial influence of far-field stresses. Obviously it cannot describe the full spectrum of possible volcano-tectonic interactions (Rowland et al. 2010), and drastic changes in eruption conditions that lead to short-term fluctuation in MER. As more reliable constraints on fissure-fed explosive eruptions become available our results may become very useful to map potential eruption mechanics or to explore alternative ways to achieve high MERs.

Acknowledgements. AC, OEM and RSJS acknowledge NERC Grant (NE/C509958/1) and support from the Royal Society International collaboration fund. RSJS acknowledges a Royal Society-Wolfson Merit Award and a European Research Council Advanced Grant. OEM acknowledges support from Russian Foundation for the Basic Research (08-01-00016). JG acknowledges support from the Royal Society URF scheme and NERC (NE/G01843X/1). T. Menand is warmly acknowledged for very useful and fruitful discussions. We thank S. Powell who helped us in preparing Figure 1 and V.C. Smith for her useful suggestions. Careful comments and criticisms by reviewers C. Wilson and S. Self led to a substantial improvement of the manuscript.

Appendix 1

Here we compare the tensile stress values along the conduit (along the *z*-axis and at a distance $c_{ch}/2$ from it) obtained using the analytical solution reported by Gao (1996) with the numerical results from a full 3D simulation obtained using COMSOL for the case of an ellipsoidal magma chamber having a spherical cross-section with a_{ch}=b_{ch}=4 km and c_{ch}=15 km. We compared the solutions with and without the effects of a free surface at a distance L of the magma chamber top. The comparison clearly shows that the 2D analytical solution is a good approximation for a first-

318 order analysis although it tends to over-estimate the tensile stress near the magma chamber and
319 to under-estimate it near the surface.

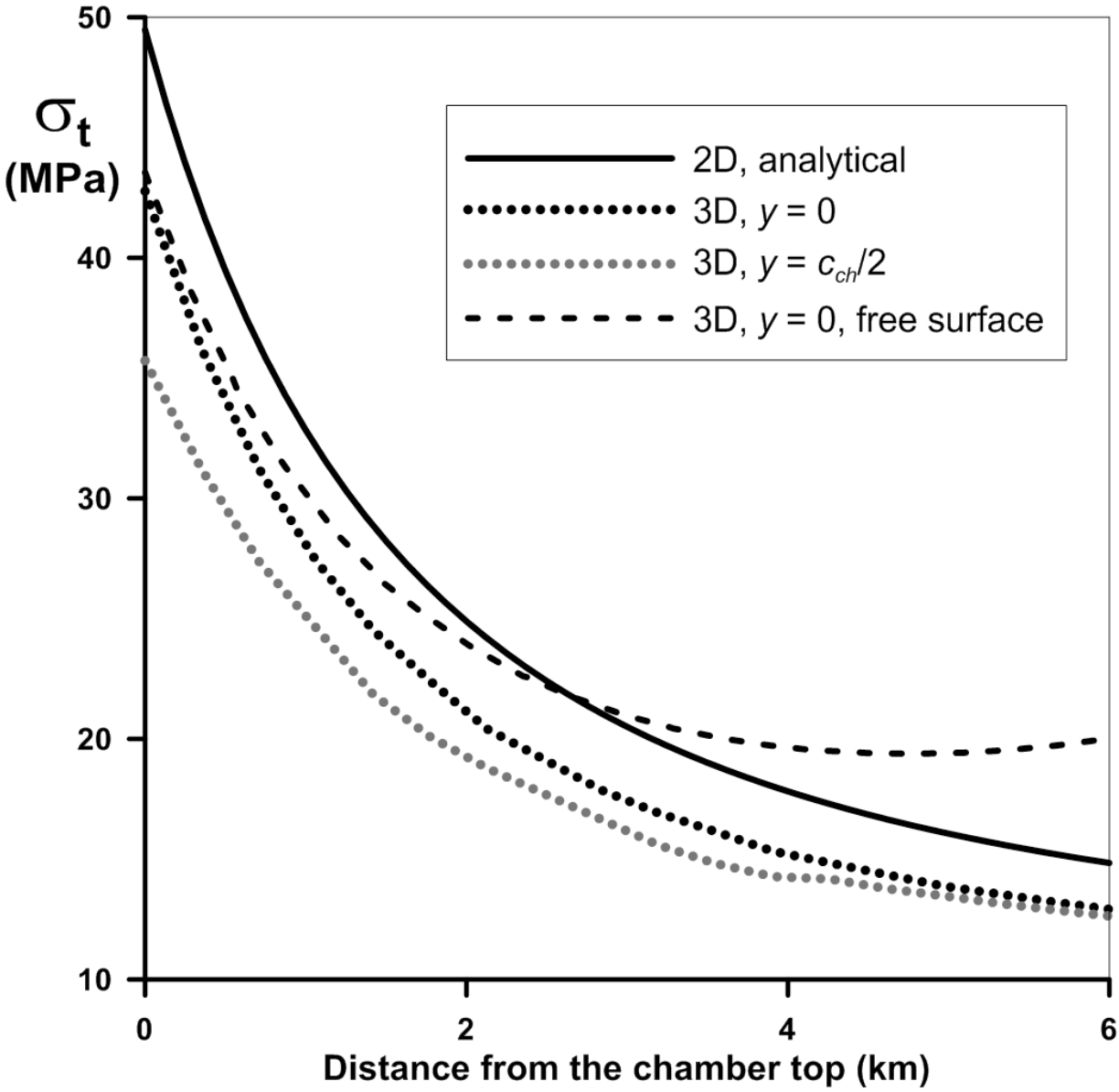

320

321 **References**

322 Aguirre-Díaz, G., Labarthe-Hernañdez, G. 2003. Fissure ignimbrites: Fissure-source origin for
323 voluminous ignimbrites of the Sierra Madre Occidental and its relationship with Basin and
324 Range faulting. Geology 31, 773-776.

325 Baines, P.G., Sparks, R.S.J., 2005. Dynamics of giant volcanic ash clouds from supervolcanic
326 eruptions. Geophys. Res. Lett. 32, L24808, doi: 10.1029/2005GL024597.

Brown, S.J.A., Wilson, C.J.N., Cole, J.W., Wooden, J., 1998. The Whakamaru group ignimbrites, Taupo Volcanic Zone, New Zealand: evidence for reverse tapping of a zoned silicic magmatic system. J. Volcanol. Geotherm. Res. 84, 1-37.

Bryan, S.E., Ferrari, L., Reiners, P.W., Allen, C.M., Petrone, C.M., Ramos-Rosique, A., Campbell, I.H., 2008. New insights into crustal contributions to large-volume rhyolite generation in the mid-Tertiary Sierra Madre Occidental province, Mexico, revealed by U-Pb geochronology. J. Petrol. 49, 47-77.

Bryan, S.E., Peate, I.U., Peate, D.W., Self, S., Jerram, D.A., Mawby, M.R., Marsh, J.S., Miller, J.A., 2010, The largest volcanic eruptions on Earth. Earth-Science Reviews, 102, 207-229.

Carey, S.N., Sparks, R.S.J., 1986. Quantitative models of the fall-out and dispersal of tephra from volcanic eruption columns. Bull. Volcanol. 48, 109-126.

Cole, J.W., Spinks, K.D., Deering, C.D., Nairn, I.A., and Leonard, G.S., 2010, Volcanic and structural evolution of the Okataina Volcanic Centre; dominantly silicic volcanism associated with the Taupo Rift, New Zealand: Journal of Volcanology and Geothermal Research, 190: 123-135.

Costa, A., Melnik, O., Vedeneeva, E., 2007a. Thermal effects during magma ascent in conduits. J. Geophys. Res. 112, doi:10.1029/2007JB004985.

Costa, A., Melnik, O., Sparks, R.S.J., 2007b. Controls of conduit geometry and wallrock elasticity on lava dome eruptions. Earth Planet. Sci. Lett. 260, 137-151, doi: 10.1016/j.epsl.2007.05.024.

Costa, A., Sparks, R.S.J. Macedonio, G., Melnik, O., 2009. Effects of wall-rock elasticity on magma flow in dykes during explosive eruptions. Earth Planet. Sci. Lett. 288, 455-462, doi: 10.1016/j.epsl.2007.05.024.

Fierstein, J., Hildreth, W., 1992. The Plinian eruptions of 1912 at Novarupta, Katmai National Park, Alaska. Bull. Volcanol. 54, 646-684.

352 Fierstein, J., Wilson, C.J.N., 2005. Assembling an ignimbrite: compositionally defined packages
353 in the 1912 Valley of Ten Thousand Smokes ignimbrite, Alaska. Geol. Soc. Am. Bull. 117,
354 1094-1107
355 Froggatt, P.C., Nelson, C.S., Carter, L., Griggs, G., Black, K.P., 1986. An exceptionally large
356 late Quaternary eruption from New Zealand. Nature 319, 578-582.
357 Gao, X.-L., 1996. A general solution of an infinite elastic plate with an elliptic hole under biaxial
358 loading. Int. J. Pres. Ves. Piping 67, 95-104.
359 Gottsmann, J., Lavallée, Y., Marti, J., Aguirre-Díaz, G., 2009. Magma–tectonic interaction and
360 the eruption of silicic batholiths. Earth Planet. Sci. Lett. 284, 426-434.
361 Gudmundsson, A., 1988. Effect of tensile stress concentration around magma chambers on
362 intrusion and extrusion frequencies. J. Volcanol. Geotherm. Res. 35, 179-194.
363 Gudmundsson, A., 1998. Formation and development of normal-fault calderas and the initiation
364 of large explosive eruptions. Bull. Volcanol. 60, 160-170.
365 Gudmundsson, A., 2002. Emplacement and arrest of sheets and dykes in central volcanoes. J.
366 Volcanol. Geotherm. Res. 116, 279-298.
367 Hautmann S., Gottsmann J., Sparks R.S.J., Costa A., Melnik O., Voight B., 2009. Modelling
368 ground deformation response to oscillating overpressure in a dyke conduit at Soufriere Hills
369 Volcano, Montserrat. Tectonophysics 471, 87-95, doi:10.1016/j.tecto.2008.10.021.
370 Hildreth, W., Mahood, G.A., 1986. Ring-fracture eruption of the Bishop Tuff. Geol. Soc. Am.
371 Bull. 97, 396-403.
372 Houghton, B.F., Carey, R.J., Cashman, K.V., Wilson, C.J.N., Hobden, B.J., Hammer, J.E., 2010.
373 Diverse patterns of ascent, degassing, and eruption of rhyolite magma during the 1.8 ka Taupo
374 eruption, New Zealand: evidence from clast vesicularity. J. Volcanol. Geotherm. Res. 195, 31-
375 47.
376 Huppert, H.E., Woods, A.W., 2002. The role of volatiles in magma chamber dynamics, Nature,
377 420, 493 – 495.

Jellinek, A.M., De Paolo, D.J., 2003. A model for the origin of large silicic magma chambers: precursors of caldera-forming eruptions. Bull. Volcanol. 65, 363-381.

Komuro, H., Fujita, Y., Kodama, K., 1984. Numerical and experimental models on the formation mechanism of collapse basins during the Green Tuff orogenesis of Japan. Bull. Volcanol. 47, 649–666.

Korringa, M.K., 1973. Linear vent area of the Soldier Meadow Tuff, an ash-flow sheet in northwestern Nevada. Geol. Soc. Am. Bull. 84, 3849-3866.

Macedonio, G., Neri, A., Martí, J., Folch, A., 2005. Temporal evolution of flow conditions in sustained magmatic explosive eruptions. J. Volcanol. Geotherm. Res. 143, 153-172, doi:10.1016/j.jvolgeores.2004.09.015.

Mason, B.G., Pyle, D.M., Oppenheimer, C., 2004. The size and frequency of the largest explosive eruptions on Earth. Bull. Volcanol. 66, 735-748.

Matthews, N.E., Pyle, D.M., Smith, V.C., Wilson, C.J.N., Huber, C., van Hinsberg, V., 2011. Quartz zoning and the pre-eruptive evolution of the ~340 ka Whakamaru magma systems, New Zealand. Contr. Mineral. Petrol, DOI: 10.1007/s00410-011-0660-1, in press.

Melnik, O., 1999. Fragmenting magma. Nature 397, 394-395.

Mériaux, C., Jaupart, C., 1995. Simple fluid dynamics models of volcanic rift zones. Earth Planet. Sci. Lett. 136, 223-240.

Miller, C., Wark, D., Self, S., Blake, S., John, D., 2008. (Potentially) Frequently asked questions about supervolcanoes and supereruptions. Elements 4, 16.

Nairn, I.A., 1992, The Te Rere and Okareka eruptive episodes - Okataina volcanic center, New Zealand. New Zeal. J. Geol. Geophys., 35, 93-108.

Papale, P., 1999. Strain-induced magma fragmentation in explosive eruptions. Nature 397, 425-428.

402 Rowland, J.V., Wilson, C.J.N., Gravley, D.M., 2010. Spatial and temporal variations in magma-
403 assisted rifting, Taupo Volcanic Zone, New Zealand. J. Volcanol. Geotherm. Res. 190, 89-108,
404 doi:10.1016/j.jvolgeores.2009.05.004.
405 Reyners, M.E., 2010. Stress and strain from earthquakes at the southern termination of the Taupo
406 Volcanic Zone, New Zealand. J. Volcanol. Geotherm. Res. 190, 82-88, doi:
407 10.1016/j.jvolgeores.2009.02.016
408 Rubin, A.M., 1995. Propagation of magma-filled cracks. Annu. Rev. Earth Planet. Sci. 23, 287–
409 336.
410 Self, S., Keszthelyi, L., and Thordarson, T., 1998. The importance of pahoehoe: Annu. Rev.
411 Earth Planet. Sci. 26, 81-110.
412 Sigmundsson, F, Hreinsdottir, S, Hooper, A, Arnadottir, T, Pedersen, R, Roberts, MJ, Oskarsson,
413 N, Auriac, A, Decriem, J, Einarsson, P, Geirsson, H, Hensch, M, Ofeigsson, BG, Sturkell, E,
414 Sveinbjornsson, H and Feigl, KL., 2010. Intrusion triggering of the 2010 Eyjafjallajokull
415 explosive eruption. Nature 468, 426-430.
416 Sigurdsson, H., Carey, S., 1989. Plinian and co-ignimbrite tephra fall from the 1815 eruption of
417 Tambora volcano. Bull. Volcanol. 51, 243–270.
418 Smith, V.C., Shane, P., Nairn, I.A., 2005. Trends in rhyolite geochemistry, mineralogy, and
419 magma storage during the last 50 kyr at Okataina and Taupo volcanic centres, Taupo Volcanic
420 Zone, New Zealand, J. Volcanol. Geotherm. Res. 148, 372-406.
421 Smith, V.C., Shane, P.A., Nairn, I.A, Williams, C.M., 2006. Geochemistry and magmatic
422 properties of eruption episodes from Haroharo Linear Vent Zone, Okataina Volcanic Centre,
423 Taupo Volcanic Zone, New Zealand during the last 10 kyr, Bull. Volcanol. 69, 57-88.
424 Sparks, R.S.J., 1978. The dynamics of bubble formation and growth in magmas: A review and
425 analysis. J. Volcanol. Geotherm. Res. 3, 1-37.

426 Sparks, R.S.J., 1986. The dimensions and dynamics of volcanic eruption columns. Bull.
427 Volcanol. 48, 3–15.
428 Suzuki-Kamata, K., Kamata, H., Bacon, C.R., 1993. Evolution of the caldera-forming eruption at
429 Crater Lake, Oregon, indicated by component analysis of lithic fragments. J. Geophys. Res. 98,
430 14059-14074.
431 Suzuki, Y.J., Koyaguchi, T., 2009. A three-dimensional numerical simulation of spreading
432 umbrella clouds. J. Geophys. Res. 114, B03209, doi:10.1029/2007JB005369.
433 Tait, S., Jaupart, C., Vergniolle, S., 1989. Pressure, gas content and eruption periodicity of a
434 shallow, crystallising magma chamber. Earth Planet. Sci. Lett. 92, 107-123.
435 Turcotte, D. L., Schubert, G. 2002. Geodynamics, 2nd edition, Cambridge University Press,
436 Cambridge.
437 Wilson, C.J.N., 1985. The Taupo eruption, New Zealand II. The Taupo ignimbrite. Phil. Trans.
438 Roy. Soc. London, A 314, 229-310.
439 Wilson, C.J.N., 2001. The 26.5 ka Oruanui eruption, New Zealand: an introduction and
440 overview. J. Volcanol. Geotherm. Res. 112, 133-174.
441 Wilson, C.J.N., 2008. Supereruptions and supervolcanoes: processes and products. Elements 4,
442 29-34.
443 Wilson, C.J.N., Gravley, D.M., Leonard, G.S., Rowland, J.V., 2009. Volcanism in the central
444 Taupo Volcanic Zone, New Zealand: tempo styles and controls. In: T. Thordarson, Self, S.,
445 Larsen, G., Rowland, S.K., Hoskuldsson, A. (Editors), Studies in Volcanology: The Legacy of
446 George Walker. Special Publications of IAVCEI 2, 225-247.
447 Wilson, L., Sparks, R.S.J., Walker, G.P.L., 1980. Explosive volcanic eruptions, IV, The control
448 of magma properties and conduit geometry on eruption column behaviour. Geophys. J. R.
449 Astron. Soc. 63, 117–148.

Wilson, C.J.N., Hildreth, W., 1997. The Bishop Tuff: New insights from eruptive stratigraphy. J. Geology 105, 407-439.

Wilson, C.J.N., Walker, G.P.L., 1981. Violence in pyroclastic flow eruptions. In: S. Self R.S.J. Sparks (Editors), Tephra Studies. D. Reidel, Dordrecht, Netherlands, pp. 441-448

Woods, A.W., Bower, S.M., 1995. The decompression of volcanic jets in a crater during explosive volcanic eruptions. Earth Planet. Sci. Lett. 131, 189-205.

CAPTION FIGURES:

Fig. 1. Sketch of the investigated system. The magma chamber having a pressure P_{ch} and a roof placed at a depth L, is assumed to be an ellipsoid with semi-axes a_{ch}, b_{ch} and c_{ch} (*i.e.,* $2a_{ch}$, $2b_{ch}$ and $2c_{ch}$ denote the width, the height and the elongation of the magma chamber respectively). Here we consider the case $a_{ch} = b_{ch}$ only. The dyke cross-section is assumed to be elliptical with a finite length $2a_d$ (along the *y*-direction) and width $2b_d$ (along the *x*-direction).

Fig. 2. a) Dyke tensile stress σ_t profile along the vertical axis obtained using the analytical solution presented by Gao (1996) for a pressurized magma chamber under the effect of different far-field extensional stresses. Values of between 0 and 60 MPa of the far-field stresses σ_{ff} were considered for a circular cross-sectional magma chamber. Gray line represents the lithostatic pressure. For σ_{ff} of 40 MPa or larger the dyke remains open throughout its entire length and dynamics are mainly controlled by the 3D geometry and extension of the system. b) Effect of crustal extension on the normalized cross-section (b_d/b_{d0}) of the dyke for the case of the

maximum sustainable dyke length for a magma chamber with a circular cross-section. For σ_{ff} larger than 40 MPa, the local tensile stresses produced by a pressurized magma chamber under the effect of an extensional far-field stress σ_{ff} result in conditions whereby the dyke can initiate and remain open despite the dramatic reduction in cross-sectional area at the fragmentation level. For both Figures magma chamber depth was fixed at *L*=6 km and magma chamber pressure was set to 20 MPa above lithostatic pressure at *L*=6 km.

Fig. 3. Maximum Eruption Rate (MER) as a function of extensional stress σ_{ff} for a dyke thickness of $b_{d0} = 5\,\mathrm{m}$ for magma chambers at 4, 6 and 8 km depth and overpressures above lithostatic of 20 MPa, respectively.

TABLES: Table 1. Parameters used.

Notation	*Description*			*Value*
x_{tot}	Concentration of dissolved gas (wt%)			5
L	Reference conduit lengths (km)			4 – 8
ρ_{l0}	Density of the melt phase (kg m^{-3})			2300
ρ_{c0}	Density of crystals (kg m^{-3})			2700
ρ_r	Host rock density (kg m^{-3})			2600
T	Magma temperature (K)			1073
x_c	Crystal fraction (wt.)			0.5
μ	Effective Magma viscosities (Pa s)			10^7
P_{ch}	Magma chamber pressure (MPa)	Depth km	L=4	122
		Depth km	L=6	173
		Depth km	L=8	224
s	Solubility coefficient ($Pa^{-1/2}$)			$4.1 \cdot 10^{-6}$
n	Solubility exponent			0.5
E_D	Dynamic rock Young modulus (GPa)			40.0
G	Static host rock rigidity (GPa)			6.0
ν	Poisson ratio			0.3
β	Bulk modulus of melt/crystal (GPa)			10
a_{ch}	Magma chamber half-width (km)			4.0
b_{ch}	Magma chamber half-height (km)			4.0
c_{ch}	Magma chamber half-elongation (km)			15
σ_{ff}	Extensional far-field stress (MPa)			0-80

496

Research Highlights

> We modelled effects of crustal extension on intensity of explosive eruptions.

> We show the control of extensional stress in sustaining dyke-fed explosive eruptions with huge mass fluxes.

> This permits huge amounts of magma to be erupted over few days through a dyke favouring conditions for column collapse.

Figure 1
Click here to download Figure: fig1.pdf

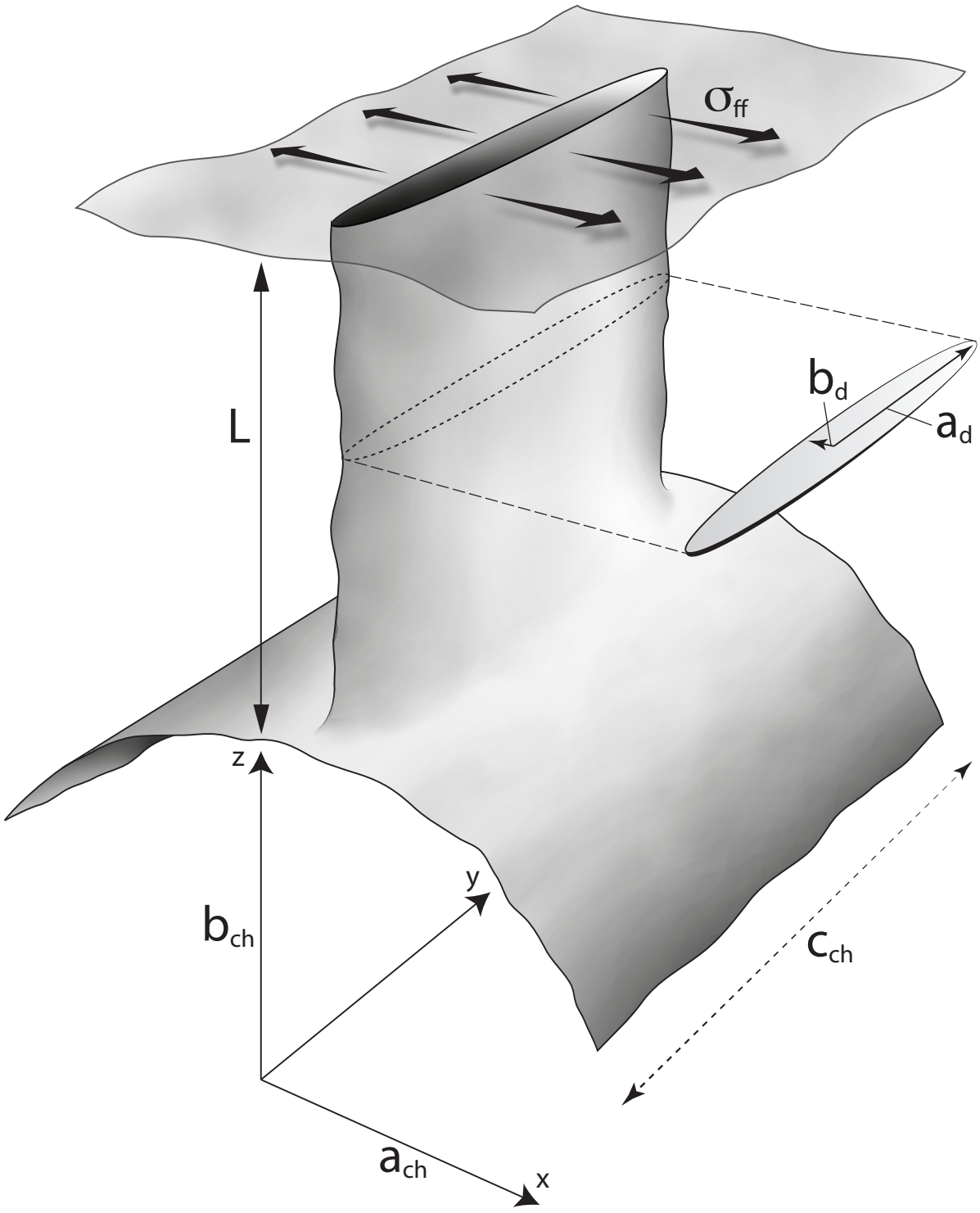

Figure 2
Click here to download Figure: fig2.pdf

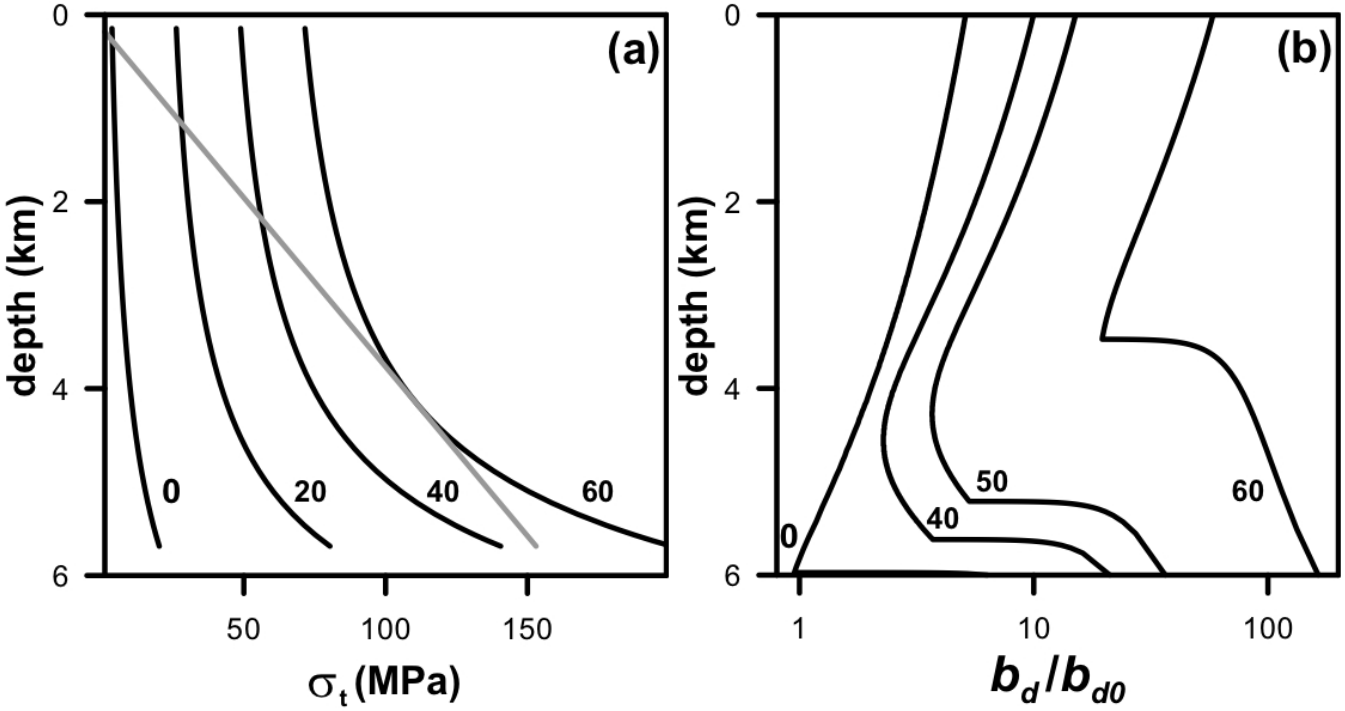

Figure 3

Click here to download Figure: fig3.pdf